Thermal lens spectrometry reveals thermo-optical property tuning of conjugated polymer nanoparticles prepared by microfluidics

Thais F. Abelha[†ab]*, Jesús Calvo-Castro*[c]*, Sandro M. Lima*[d]*, Júnior R. Silva*[d]*, Luis Humberto da Cunha Andrade*[d]*, John C. de Mello*[e]*, Cécile A. Dreiss*[b]*, Mark Green*[f] *and Lea Ann Dailey*[g]

[a] Federal University of Mato Grosso do Sul, Institute of Physics, Campo Grande, Mato Grosso do Sul, 79070-900, Brazil. E-mail: thais.abelha@ufms.br

[b] King's College London, Institute of Pharmaceutical Science, 150 Stamford Street, SE1 9NH, London, UK.

[c] University of Hertfordshire, School of Life and Medical Sciences, AL109AB, Hatfield, UK.

[d] Universidade Estadual de Mato Grosso do Sul, Grupo de Espectroscopia Óptica e Fototérmica, Dourados, Mato Grosso do Sul, 79804-970, Brazil. E-mail: smlima@uems.br

[e] Department of Chemistry, Norwegian University of Science and Technology (NTNU), 7491 Trondheim, Norway

[f] Department of Physics, King's College London, Strand Campus, WC2R 2LS, London, UK.

[g] University of Vienna, Dept. of Pharmaceutical Sciences,y, Althanstr. 14, 1090 Vienna, Austria.

Keywords: Conducting polymers, microfluidics, nanoparticles, thermal lens spectroscopy, light-to-heat conversion efficiency

ABSTRACT: Conjugated polymers display useful thermo-optical properties of high relevance to biomedical applications, which are not only dependent on their intrinsic chemical composition, but also related to their physical conformation and manufacturing protocol. In this work we report that the thermo-optical properties of poly[2,6-(4,4-bis-(2-ethylhexyl)-4H-cyclopenta[2,1-b;3,4-b']dithiophene)-alt-4,7(2,1,3-benzothiadiazole)] (PCPDTBT) encapsulated within poly (ethylene glycol) methyl ether-block-poly (lactide-co-glycolide) (PEG-PLGA) can be tuned by production conditions, generating conjugated polymer nanoparticles (CPNs) with customized applications. Thermal lens spectroscopy (TLS) was used to characterize the CPN light-to-heat conversion efficiency as it provides an absolute measurement of heat generation. Although preparation by traditional bulk production led to a high product yield, the CPNs were characterized by similar sizes and thermo-optical properties, irrespective of the molecular weight of amphiphilic PEG-PLGA. In contrast, a microfluidics production method generated CPNs with variable product yields and sizes and thermo-optical properties that are affected both by the molecular weight of PEG-PLGA and the production settings. Given the growing interest in biomedical applications of CPNs, our work provides useful results on microfluidic production of CPNs and of TLS for the screening of candidates with desirable characteristics.

INTRODUCTION

Conjugated polymers (or semiconducting polymers) are organic materials that present useful electronic and optical properties with a broad range of technological applications.[1–3] Within

the biomedical field, their photoluminescence emission and photoacoustic signal have been explored for bioimaging,[3] while their light-triggered reactive oxygen species (ROS) and heat generation capabilities have been used for photodynamic (PDT) and photothermal therapies (PTTs) for cancer and bacterial infections.[2,4,5] The useful properties of conjugated polymers depend on their inherent chemical structure and degree of polymerization, as well as on their physical conformation.[1,6–8] Because of the latter, both the conditions of preparation [9] and the type of amphiphilic compounds used for their dispersion in aqueous solutions[10] have a direct impact on their performance. As a consequence, these factors can be used to optimize the characteristics of conjugated polymer nanoparticles (CPNs) for the application sought. As the potential application of conjugated polymers depends on the mechanisms of energy dissipation following excitation, the study of the radiative and non-radiative de-excitation mechanisms is paramount for the identification of candidates with enhanced properties. This could inform the choice of preparation conditions to generate nanoparticles suitable for specific types of instrumentation.

The commercially available conjugated polymer poly[2,6-(4,4-bis-(2-ethylhexyl)-4H-cyclopenta[2,1-b;3,4-b']dithiophene)-*alt*-4,7(2,1,3-benzothiadiazole)] (PCPDTBT) (**Figure 1**) is a biocompatible material[10] that has been explored for biomedical applications due to its light absorption and emission in the near infrared region and its capability of heat/sound wave generation.[11–13] Hence, PCPDTBT nanoparticles have been used both as photoacoustic[11–13] and fluorescent[11,12] bioimaging probes and as a cytotoxic photothermal agent.[12] The literature suggests that PCPDTBT CPNs can emit detectable light and acoustic/thermal waves and that the performance of PCPDTBT CPNs in biomedical applications is linked to the extent of light and heat generated.[11,13] The optical properties and photoacoustic effect of PCPDTBT nanoparticles have been characterized with diverse techniques and contrasting outcomes in their performance

have been observed.[11–13] For example, PCPDTBT nanoparticles stabilized with the surfactant 1,2-dipalmitoyl-*sn*-glycero-3-phosphocholine (DPPC) presented 0.1% fluorescence quantum yield,[11] determined by the relative method,[14–16] while higher fluorescence efficiencies (39%) were reported for CPNs prepared with 1,2-dioctanoyl-*sn*-glycero-3-phosphocholine (DOPC) lipid (fluorescence quantum yield method not described).[12]

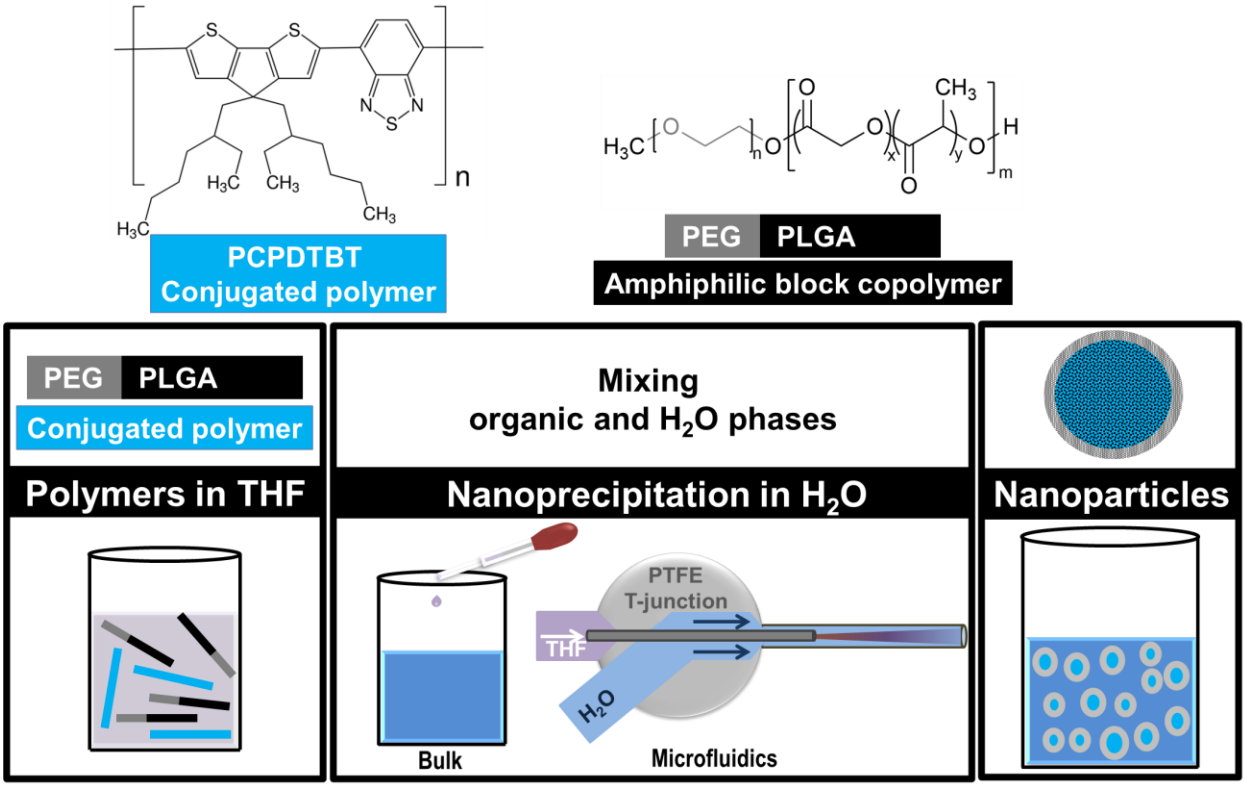

Figure 1. PCPDTBT and PEG-PLGA chemical structures and nanoparticle preparation settings.

When assessing the photothermal effects of PCPDTBT, the photoacoustic characterization has been typically performed using an ultrasound detector,[11,13] although one report employed photothermal optical coherence tomography.[12] Ultrasound detectors [11,13,17] used for photoacoustic measurements make use of a microphone to monitor the thermal effect caused by non-radiative

de-excitation,[18] relying on the principle that the absorbed photon energy is converted into an acoustic signal.[18] However, there are other photothermal methods used to measure the thermal effect created in a sample due non-radiative de-excitation, such as thermal lens spectrometry (TLS), photothermal deflection spectrometry and thermal mirror spectrometry, which vary in the principles followed to measure the amount of absorbed energy converted into heat.[19] First described in 1965, TLS (also referred to as thermal lensing) is based on the detection of heat produced following photoexcitation (photothermal effect).[20,21] Briefly, in the TLS method, a local change in refractive index due to the absorption of light from a pump beam can interfere in the plane wave of a second laser (probe beam), observed as a defocusing with an associated drop in the centre of the probe beam intensity. The temperature change within the sample due to the pump beam can be calculated from the change in the probe beam intensity, and it is related to the thermo-optical properties of the sample. TLS provides an absolute measurement of heat generation and has the advantage of using a laser instead of a xenon lamp as a light source, which replicates more closely the excitation conditions often used in biomedical applications.[22]

In this work, PCPDTBT CPNs containing amphiphilic block copolymers of poly (ethylene glycol) methyl ether-block-poly (lactide-co-glycolide) of different molecular weights (PEG_{2k}-$PLGA_{15k}$ and PEG_{5k}-$PLGA_{55k}$) were produced by a traditional bulk technique and microfluidics (**Figure 1**). TLS was used to characterize the thermo-optical properties of CPNs in order to understand the effect of the molecular weight of PEG-PLGA and the production techniques on PCPDTBT physical conformation within the nanostructure, enabling informed preparation conditions for CPNs with tailored thermo-optical properties. In short, we observe that the traditional bulk technique generated high product yields of PCPDTBT CPNs with similar optical and thermal properties and sizes, regardless of the PEG-PLGA molecular weight. In contrast, it is

of note that the size and thermo-optical properties of PCPDTBT-based CPNs can be tailored by means of microfluidics production.

EXPERIMENTAL SECTION

1. Materials

PCPDTBT (cat # 754005) with an average molecular weight of 7482 Da; two different types of poly (ethylene glycol) methyl ether-block-poly (lactide-co-glycolide) copolymers with 50:50 ratio of lactide:glycolide (PEG_{2k}-$PLGA_{15k}$ and PEG_{5k}-$PLGA_{55k}$); THF (ReagentPlus®, ≥99.0%, cat # 178810); purified HPLC water (impurities ≤1ppb and anions ≤ 0.1 mg/Kg, cat # 34877-2.5L); Cheminert® PTFE plastic fittings and tubing and 5 mL glass syringe with 10.301 mm diameter (21965-U, Supelco) were supplied by Sigma-Aldrich Corporation (St Louis, MO, USA). Synthetic fused silica capillary tubing TSP320450 and TSP100245 was supplied by (Polymicro Technologies LLC, Phoenix, Arizona, USA). Syringe pumps 11 Elite Infusion Only Single Syringe (cat # 70-4500) were acquired from Harvard Apparatus (Massachusetts, USA).

2. Nanoparticle preparation

Nanoparticles were prepared with a mass ratio of 1:20 (PCPDTBT:PEG-PLGA) through nanoprecipitation using a bulk method and a continuous fabrication technique (microfluidics) (**Figure 2**), both previously used to prepare PEG-PLGA CPNs containing conjugated polymers of variable structures.[9,10]

2.1 Bulk method

PCPDTBT bulk formulations were prepared with total solids concentrations of 2.1 mg/mL in the end product. THF (1 mL) containing 10.5 mg/mL total polymer (5% w/w conjugated

polymer and 95% PEG-PLGA) was added dropwise to 5 mL of water at room temperature stirred for up to 12 hours to allow complete evaporation of THF. The volume of water lost due to evaporation was replaced. Corresponding formulations containing 100% PEG_{2k}-$PLGA_{15k}$ and PEG_{5k}-$PLGA_{55k}$ were prepared as controls with 2.0 mg/mL final polymer concentration. At least three independent replicate batches of each formulation were produced and characterized.

2.2 Microfluidics

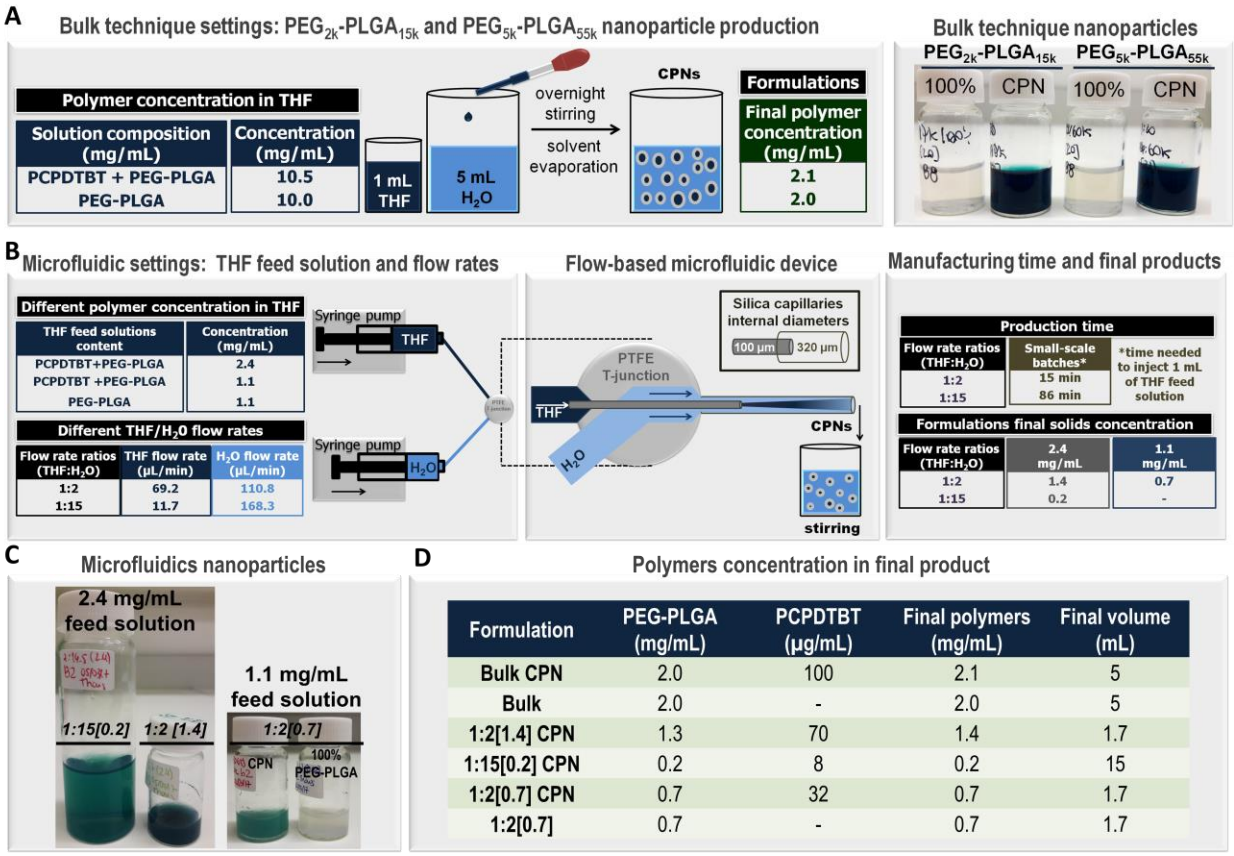

Formulation	PEG-PLGA (mg/mL)	PCPDTBT (µg/mL)	Final polymers (mg/mL)	Final volume (mL)
Bulk CPN	2.0	100	2.1	5
Bulk	2.0	-	2.0	5
1:2[1.4] CPN	1.3	70	1.4	1.7
1:15[0.2] CPN	0.2	8	0.2	15
1:2[0.7] CPN	0.7	32	0.7	1.7
1:2[0.7]	0.7	-	0.7	1.7

Figure 2. Illustration of the production settings of the bulk method (A) and microfluidic CPN production (B/C). PDPCTBT CPNs were produced at (5% w/w conjugated polymer and 95% PEG-PLGA) (D).

The same microfluidic device previously used for both small and large-scale batch production of PEG-PLGA CPNs[9] was used to prepare PCPDTBT nanoparticles. Nanoparticles

were prepared by injecting a fixed volume of 1 mL of THF polymer feed solution, leading to formulations which varied in their final volume depending on the flow rate ratio of THF to water used (**Table 1**). The nanoparticles were collected in a flask and were stirred continuously for up to 12 hours to allow complete evaporation of THF and the volume of water lost due to evaporation was replaced. Nanoparticles were prepared at the highest and lowest polymer concentrations previously reported.[9] At least three independent replicate batches of each formulation were produced and characterized.

Table 1. Experimental conditions investigated to prepare nanoparticles in a continuous process (microfluidics).

Feed solution concentration	THF flow rate (µL/min)	H_2O flow rate (µL/min)	Flow rate ratio (THF:H_2O)*	Total solids concentration in product [mg/mL]	CPN abbreviation
2.4 mg/mL (5% PCPDTBT: 95% PEG-PLGA)	69	111	1:2	1.4	1:2[1.4]
	12	168	1:15	0.2	1:15[0.2]
1.1 mg/mL (5% PCPDTBT: 95% PEG-PLGA)	69	111	1:2	0.7	1:2[0.7]
1.1 mg/mL (100% PEG-PLGA)	69	111	1:2	0.7	1:2[0.7] 100%PEG-PLGA

*For clarity, the flow rate ratios have been rounded to the nearest integer or half integer in abbreviations used for the text and figures.

3. Product yield

The product yield (PCPDTBT concentration in a defined volume of CPN solution expressed as a percentage of the theoretical concentration of conjugated polymer assuming zero loss) was determined as previously described.[9] Briefly, duplicate samples (50-200 µL) of each CPN were dried in an oven and solubilized in 1 mL of THF prior to absorbance measurements. PCPDTBT calibration curves were prepared in THF in the concentration range of 0.8-12.5 µg/mL and absorbance assessed in a Lambda 35 absorption spectrophotometer (Perkin Elmer Inc., USA) at 700 nm.

4. Optical and thermal characterization by thermal lens spectrometry (TLS)

For TLS characterization, CPNs and 100% PEG-PLGA nanoparticles were assessed at total solids concentration of 3, 30 and 300 µg/mL. The TLS experimental setup was performed with a dual-beam mode-mismatched configuration (Figure S1), as previously described.[23] Briefly, samples were presented using 1 mm quartz cuvettes, and placed at the minimum position of the beam waist (w_{oe}) of a Ti^{3+}:Sapphire laser pumped by a semiconductor laser with λ = 532 nm. The excitation was performed by the Ti^{3+}:Sapphire laser tuned at 700 nm and the thermal lens (TL) effect was probed by a HeNe laser operating in 632.8 nm. The excitation beam has a Gaussian intensity profile, whereby when it passes through the sample, a change in the refractive index is locally induced, which is proportional to the temperature change. The probe beam also has a Gaussian intensity profile and constantly impinges the sample, but it has much lower potency and its diameter is about five times larger than the excitation beam. Accordingly, it does not induce any temperature change in the sample. A similar instrumentation set up was previously used for the quantum yield determination of solid samples of Nd^{3+}-doped low silica calcium aluminate glasses,[24] Yb^{3}-doped tellurite glasses,[25] Er^{3+}-doped tellurite glasses,[26] and in liquid samples of

rhodamine 6G and diketopyrrolopyrrole based materials.[27] The samples were pumped by intermittent light for 450 ms and no photoreaction was observed with the excitation at 700 nm.

It was important to determine if the PEG-PLGA component had any effect on the properties of the CPNs studied. Therefore 100% PEG-PLGA nanoparticles prepared by the bulk technique were evaluated with regards to their thermal diffusivity and their thermal lens effect amplitude. By fitting the TL characteristic curves (**Figure S2**), the TL time response, t_c, is obtained. In order to determine the thermal diffusivity of the samples, the relation $D = (w_{oe})^2/4t_c$ was used and the thermal diffusivity values obtained in samples with three different nanoparticle concentrations (300, 30 and 3 μg/mL total solids) were compared to accepted reports of water characterization.[28,29] The thermal diffusivity of PEG-PLGA nanoparticles without PCPDTBT was $(1.42 \pm 0.09)\times10^{-3}$ cm^2/s, independent of the concentrations tested, and matched the value of water, meaning that the PEG-PLGA on its own would not contribute to the thermal lens effect. The TL effect amplitude was the same for all samples studied (**Figure S3**), reinforcing that only pure water is contributing to the thermal lens effect. Similar results were obtained for both PEG-PLGA nanoparticles regardless of polymer molecular weight.

For the TLS characterization, it is necessary to determine a linearity of fit based on the thermal lens signal amplitude under different laser powers. A linear relationship was observed for all CPN samples and is depicted using a representative sample, microfluidics 1:2[1.4] containing PEG_{5k}-$PLGA_{55k}$ (**Figures S4**). The linear behaviour indicates that during the sample excitation with the laser only the thermal lens effect is responsible for the acquired signal.

5. Hydrodynamic diameter and zeta potential determination

Hydrodynamic diameters were assessed by dynamic light scattering (DLS) at 25°C using a Zetasizer NanoZS (Malvern Instruments Ltd, UK) equipped with a 633 nm He-Ne laser and a back scatter detector with measurement angle of 173°. The size analysis was performed at 50 µg/mL total solids concentration. The Z-average value obtained from the intensity distribution of particles size was used to express the mean diameters of monomodal samples. For zeta potential measurements, CPNs were diluted in NaCl 10 mM [30,31] at a final polymer concentration of 20 µg/mL, and the measurements were performed in standard electrophoresis cuvettes (DTS1070, Malvern Instruments GmbH) in a Zetasizer NanoZS (Malvern Instruments Ltd, UK) equipped with a 633 nm He-Ne laser and forward scatter detector with a measurement angle of 13º.

6. Steady-state absorption and fluorescence emission spectra

Steady-state absorption and fluorescence emission spectra of PCPDTBT dissolved in THF and nanoparticles diluted in water at concentrations of 0.2-12.5 µg/mL PDPCTBT were measured using a Lambda 35 absorption spectrophotometer (Perkin Elmer Inc., USA) and a LS50b luminescence spectrometer (Perkin Elmer Inc., USA), respectively. The average absorbance/emission spectrum of at least three independent nanoparticle batches was calculated and then maximum-normalized. The attenuation coefficient (formerly known as extinction coefficient, $cm^{-1}g^{-1}L$) of CPNs was determined as previously described for metal nanoparticles. [32–34] Briefly, these attenuation coefficients were determined from the gradient of the linear ($R^2 \geq 0.994$) regression when the absorption at the relevant wavelength was plotted against concentration ($n = 5$). In all cases, and to account for the nanoparticle scattering effect, the measured absorbance values of CPNs were corrected with the values obtained of the non-absorbing 100% PEG-PLGA

nanoparticles at the same polymer concentrations. Quoted values represent average and associated uncertainty as a single standard deviation for three independent nanoparticle batches.

7. Statistical analysis

GraphPad Prism (version 5.00 for Windows, GraphPad Software, San Diego California, USA) was used to perform statistical (One-way ANOVA with Tukey's post hoc test and regression analysis) and Pearson correlation analysis. Statistical significance values were described as * $p \leq 0.05$ ** $p \leq 0.01$, *** $p \leq 0.001$.

RESULTS AND DISCUSSION

1. CPNs production yield, size and charge

The CPN product yield denotes an important parameter as it provides information about the viability of production methods that should ideally cause a minimum material loss.[9] PCPDTBT CPNs produced by the bulk method presented higher product yields than those generated by microfluidics, regardless of the molecular weight of the PEG-PLGA (**Figure 3**). The type of PEG-PLGA influenced the yield of CPNs generated via microfluidics: PEG_{5k}-$PLGA_{55k}$ CPNs presented more variable and larger mean yields (70-85%) than the nanoparticles containing PEG_{2k}-$PLGA_{15k}$ (63-74%). In addition, it is of note that the settings of the microfluidic production have a clear effect on the product yield for both systems. In this regard, reducing the polymer concentration on the THF feed solution from 2.4 to 1.1 mg/mL led to a higher product yield of PEG_{5k}-$PLGA_{55k}$

CPNs (MF1:2[0.7]), while the lowest THF:H_2O flow rate ratio generated the highest product yield of PEG_{2k}-$PLGA_{15k}$ microfluidics CPNs (MF1:15[0.2]).

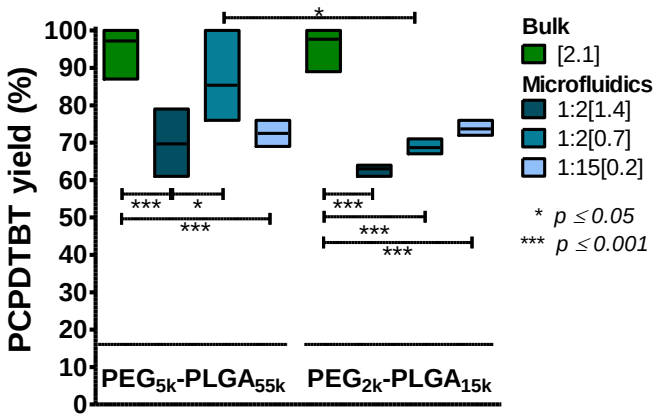

Figure 3. Product yield of PCPDTBT-based CPNs produced by the bulk and microfluidics techniques. Boxes represent minimum and maximum values with line at mean (n≥3).

Interestingly, we observed that both production techniques generated higher PCPDTBT yields than poly(9,9-dioctylfluorene-2,1,3-benzothiadiazole) (F8BT) nanoparticles prepared with the surfactants sodium dodecyl sulfate (SDS) or Solutol HS (pegylated 12-hydroxystearate) produced by miniemulsion technique (<30%)[35] and PLGA nanoparticles encapsulating the conjugated polymers poly[9,9-dihexylfluorene-alt-9,9-bis(2-(2-(2-methoxyethoxy)ethoxy)ethyl)fluorine] (PF), poly[9,9-bis(2-(2-(2-methoxyethoxy)ethoxy)ethyl)fluorenyldivinylene-alt-9,9-bis(3-t-butylpropanoate)fluorene] (PFV), poly[9,9-bis(2-(2-(2-methox-yethoxy)ethoxy)ethyl)fluorene-alt-4,7-(2,1,3-benzothiadiazol)] (PFBT), and MEH-PPV (41-48%).[36] In comparison to cyano-substituted poly(p-phenylene vinylene) (CN-PPV) and F8BT CPNs containing PEG_{5k}-$PLGA_{55k}$ produced previously with the same settings,[9] the bulk method led to higher product yields of PCPDTBT/PEG_{5k}-$PLGA_{55k}$ CPNs, while the ones obtained by microfluidics had a lower conjugated polymer content than CN-PPV, but higher than F8BT.

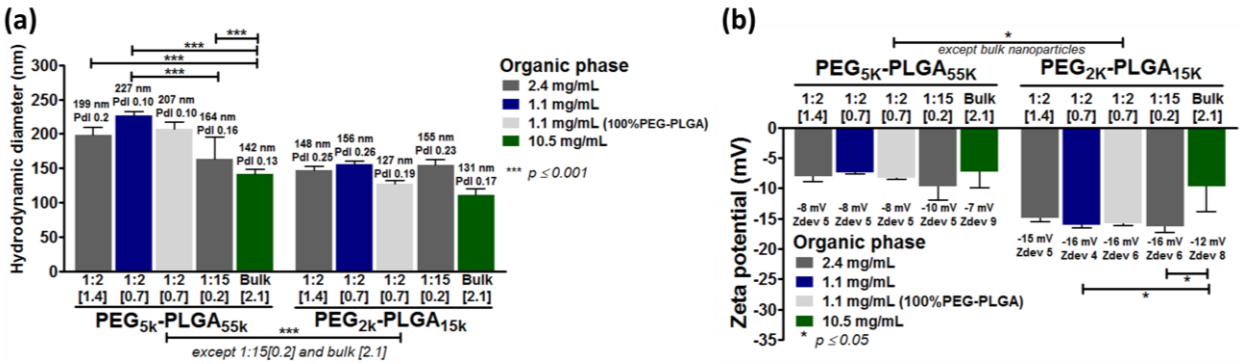

Figure 4. Hydrodynamic diameters (a) and zeta potential (b) of PCPDTBT CPNs produced by the bulk and microfluidics techniques.

We have previously shown that PCPDTBT/PEG-PLGA nanoparticle size of CPNs prepared by the bulk method is affected by the molecular weight of PEG-PLGA, the total concentration of polymers and the percentage of incorporation of PCPDTBT,[10] yielding circular shaped CPNs.[9,10] In this work, we observed that microfluidics nanoparticles containing PEG_{5k}-$PLGA_{55k}$ presented significantly ($p \leq 0.001$) larger sizes than bulk CPNs, despite their lower total solids concentration (**Figure 4a**). On the other hand, nanoparticles containing PEG_{2k}-$PLGA_{15k}$ were similar in size to formulations produced by the different techniques, but the microfluidic formulations exhibited the highest polydispersity (>0.2). In addition, nanoparticles containing PEG_{5k}-$PLGA_{55k}$ had significantly ($p \leq 0.001$) larger sizes (164-199 nm) than the PEG_{2k}-$PLGA_{15k}$ formulations (127-156 nm), except for the bulk nanoparticles and CPNs prepared with the lowest THF:H_2O flow rate ratio (1:15[0.2]) (**Figure 4a**). This outcome is in agreement with literature reports for copolymers with increasing molecular weights, such as PEG_{5k}-$PLGA_{27/55/95k}$[37] and PEG_{5k}-$PLGA_{10/27/45/95k}$,[38] which generated nanoparticles of increasing sizes under the same production conditions in flow focusing microfluidic devices.

In addition to the size, the surface properties of nanoparticles designed for biomedical applications have an important effect on their circulation, distribution and cellular internalization.[39,40] It is worth mentioning that PCPDTBT CPNs stabilized with both PEG_{2k}-$PLGA_{15k}$ and PEG_{5k}-$PLGA_{55k}$ assessed previously presented excellent biocompatibility with mammalian cells and human blood components and showed stable properties in relevant biological media.[10] The zeta potential is related to the different material composition of a formulation, with the end groups on the nanoparticle surface influencing the charge present in each system.[41] Nanoparticles containing PEG_{5k}-$PLGA_{55k}$ presented zeta potential values close to neutral (< -10 mV)[42] irrespective of the production techniques or manufacturing settings (**Figure 4b**). This is in agreement with previous literature reports of PEG_{5k}-$PLGA_{55k}$ CPNs[9,10] and PEG_{5k}-$PLGA_{34k}$ nanoparticles.[43] PEG_{2k}-$PLGA_{15k}$ based nanoparticles prepared by microfluidics had an arguably small, but significantly more electronegative zeta potential (ca -16 mV, $p \leq 0.05$) than the bulk formulation and PEG_{5k}-$PLGA_{55k}$ CPNs. The fact that PEG_{2k}-$PLGA_{15k}$ microfluidics formulations were more electronegative than the ones prepared by the bulk method could be related to the higher polydispersity of the microfluidics nanoparticles, as the zeta potential depends on the nanoparticle size and polydispersity.[44] Despite that, all formulations presented a more neutral surface charge in comparison to non-PEGylated PLGA nanoparticles (e.g. -30 mV[36], -26 mV[45] and -40 mV[30]) and non-PEGylated PLGA nanoparticles encapsulating the conjugated polymers PF PFV, PFBT and MEH-PPV (ca -35 mV).[36]

2. Optical and thermal properties

The characterization of the optical properties of a material includes the determination of the absorption and emission spectra, attenuation coefficient and the fluorescence quantum yield.[14] These properties are also related to the photothermal characteristics, which are associated to the ability of a material to convert the absorbed energy into heat.[19] This heat generation efficiency, as well as the heat diffusion through the sample, are relevant photothermal properties of a material.[19] In this work the thermo-optical characterization of CNP formulations was carried out with particular emphasis on the evaluation of the CPNs preferential excited state de-activation mechanisms.

2.1 Absorption and fluorescence emission spectra

A solution of PCPDTBT in THF presented absorbance and emission in the near infrared (**Figure 5**), with a blue shifted maximum absorption compared to PCPDTBT dissolved in chloroform (718 nm).[12] The maximum absorbance of all CPNs showed a hypsochromic shift when compared to PCPDTBT fully solvated in THF (**Figure 5**). In confined structures, the conjugated polymers chains twist and fold, affecting the extent of the polymer conjugation length and thus HOMO-LUMO bandgaps.[36,46,47] This is consistent with our experimentally observed hypsochromic shifts in the absorption spectrum on progression from PCPDTBT polymer solutions to CPNs. In all cases, we observe broader absorption spectra for the latter, which we attribute to a wider distribution of thermodynamically accessible polymer conformations. The bulk nanoparticles had a 40 nm hypsochromic shift irrespective of the type of PEG-PLGA, while microfluidics CPNs presented absorbance blue shifts of 20 nm (PEG_{5k}-$PLGA_{55k}$) and 10 nm (PEG_{2k}-$PLGA_{15k}$), independently of production conditions. This outcome suggests that the bulk

technique led to a more tightly coiled conformation of PCPDTBT inside the compact nanostructure independent of the type of PEG-PLGA. Above all, the rapid and stable mixing conditions of microfluidic production enabled tuning the maximum absorbance of nanoparticles closer to the near infrared region.

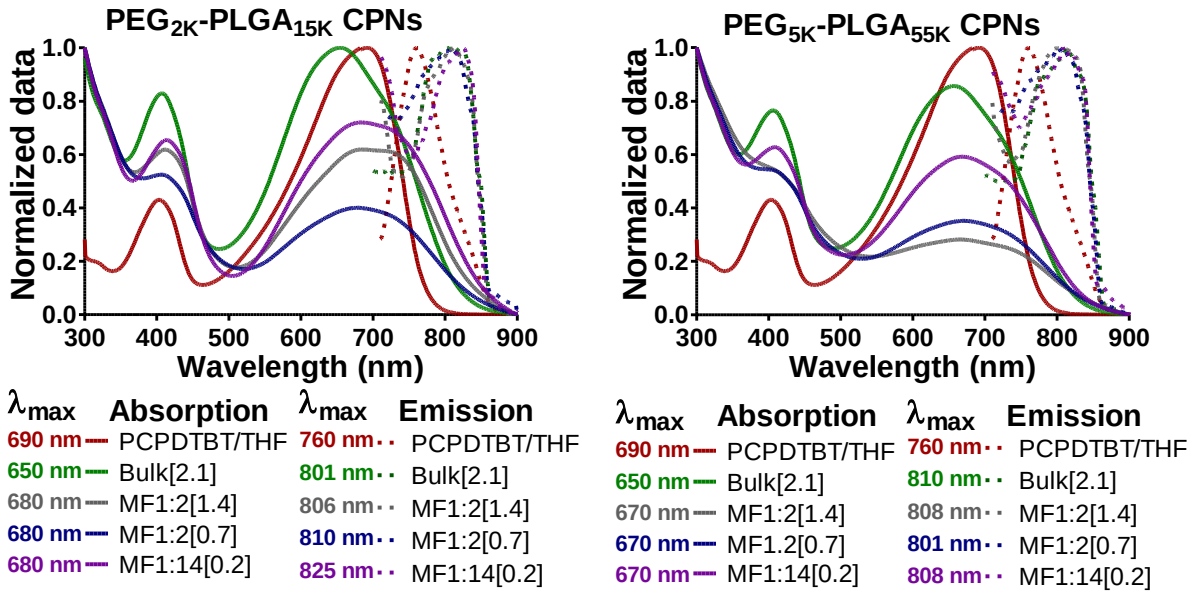

Figure 5. Normalized absorption (solid line) and fluorescence emission (dashed line) spectra of PCPDTBT in THF and PCPDTBT CPNs in water produced by the bulk and microfluidics (MF) methods.

Whilst the absorption spectrum provides insightful information in relation to, for example, excitation wavelength of choice for bio-applications, the attenuation coefficient informs about the ability of the material to absorb light at a particular wavelength. As a result, large attenuation coefficients would facilitate lower working concentrations in bio-assays. For biomedical applications, there is interest in materials that absorb and emit in the near infrared region of the spectrum (700–2500 nm), due to increased light penetration compared to lower wavelengths,

which are significantly absorbed and scattered by tissue.[48,49] In this regard, all CPNs exhibited absorption maximum at wavelengths longer than 650 nm, widely accepted as suitable for in vivo biomedical applications.[49] Nonetheless, for completeness **Table 2** summarizes experimentally determined attenuation coefficients for these formulations at their absorption maximum as well as 700 nm. In general, microfluidics CPNs produced under the highest THF:H_2O flow rate ratio (1:2) presented the largest attenuation coefficients at their absorption maximum as well as 700 nm (**Table 2**). Moreover, PEG_{5k}-$PLGA_{55k}$ CPNs generally presented higher values than PEG_{2k}-$PLGA_{15k}$ at 700 nm, but only the bulk method CPNs containing PEG_{5k}-$PLGA_{55k}$ presented significantly ($p \leq 0.05$) higher absorption coefficient than their PEG_{2k}-$PLGA_{15k}$ counterparts. In addition, all CPNs presented significantly ($p \leq 0.0001$) reduced attenuation coefficients in comparison with PCPDTBT in THF. PCPDTBT presented a higher mass attenuation coefficient in THF at 690 nm than F8BT in DCM (59.84 $cm^{-1}g^{-1}L$ at 447 nm),[50] while the CPNs prepared in this study presented similar mass attenuation coefficients to F8BT/gadolinium nanoparticles prepared with phospholipids as stabilizing agents (41.4 $cm^{-1}g^{-1}L$ at 450 nm) [51], but lower than PCPDTBT nanoparticles prepared with the surfactant DPPC (93 $cm^{-1}g^{-1}L$ at 660 nm).[11]

Table 2. Mass attenuation coefficients (α) of PCPDTBT in THF and CPNs in water at $\lambda_{max.}$ and 700 nm.

PEG-PLGA	Sample	$\lambda_{abs.max.}$ (nm)	α ($cm^{-1}g^{-1}L$)	α ($cm^{-1}g^{-1}L$) 700 nm
-	PCPDTBT	690	69±0	68±0
PEG_{2k}-$PLGA_{15k}$	Bulk[2.1]	650	44±3	37±2
	MF1:2[1.4]	680	40±2	40±2
	MF1:2[0.7]	680	46±3	45±3

	MF1:14[0.2]	680	42±6	42±1
PEG_{5k}-$PLGA_{55k}$	Bulk[2.1]	650	43±3	46±4
	MF1:2[1.4]	670	43±3	43±4
	MF1:2[0.7]	670	48±4	48±4
	MF1:14[0.2]	670	46±2	45±1

CPNs prepared by both production techniques presented a similar red-shift in the emission spectra in comparison to PCPDTBT in THF (**Figure 5**). The emission maxima of CPNs containing PEG_{2k}-$PLGA_{15k}$ were red-shifted by ca 40-65 nm, while PEG_{5k}-$PLGA_{55k}$ CPNs presented a red-shift of ca 40-50 nm. These were observed to be similar to the previously reported 62 nm red-shift for PCPDTBT nanoparticles produced with the lipid DOPC in comparison to the neat conjugated polymer chloroform solution.[12] In nanoparticle structures, the conjugated polymer chromophores are in close proximity, favoring the formation of interchain interactions, such as aggregated species,[46] resulting in red shift in the emission spectra.[46,52] It is worth noting the larger Stokes shifts for these PEG-PLGA formulations when compared to their neat PCPDTBT solutions, which represent an advantage for their application in line with smaller spectral overlap and lower probability of self-absorption.

2.2 CPN de-excitation mechanisms

We previously reported that the aqueous and organic phases mixing have an important effect on the CPNs optical properties, with microfluidic settings generating nanoparticles with tuneable fluorescence quantum yields, while bulk CPNs had similar performance regardless of polymers concentrations.[9] PCPDTBT-based formulations were characterized in relation to the

excited state de-excitation mechanism following light absorption. Molecules can undergo this process by both radiative and non-radiative mechanisms.[53,54] In order to experimentally determine the quantum yield for heat generation upon photo excitation, two important parameters, namely thermal diffusivity and heat generation were determined. These are related to the speed of heat distribution through the sample and how much of the absorbed energy is converted into heat, respectively.

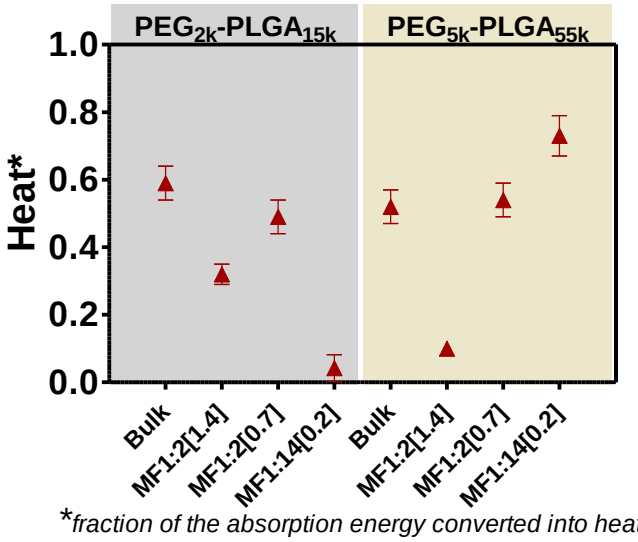

Figure 6. Fraction of the absorbed energy converted into heat of the different nanoparticles at 30 µg/mL total solids (1.4 µg/mL PCPDTBT + 28.6 µg/mL PEG-PLGA) following photoexcitation at 700 nm.

The evaluation of potential preparation-induced preferential de-excitation pathways of PCPDTBT CNPs was of particular interest. It is of note that whilst bulk CPNs were observed to exhibit comparable heat generation capabilities irrespective of molecular weight of the PEG-PLGA, different heat generation efficiencies were yielded by the ones produced by microfluidics. TLS analysis revealed the largest non-radiative de-activation efficiency for the microfluidic formulations MF1:14[0.2] in the presence of PEG_{5k}-$PLGA_{55k}$, while the opposite was observed for

PEG_{2k}-$PLGA_{15k}$ CPNs obtained under the same condition (**Figure 6**). Along these lines, we observed a significant bathochromic shift for this formulation on progression from high (λ_{em} = 808 nm) to low (λ_{em} = 825 nm) PEG-PLGA molecular weight. While these observations are consistent with the energy gap law [55] (i.e. there is an increase in the non-radiative decay rate constant as the emission energy decreases), it is also anticipated that alternative excited state de-activation pathways become available in the case of the formulation with PEG_{5k}-$PLGA_{55k}$, hence facilitating a more efficient radiation-less process. Importantly, the microfluidics technique enabled tuning CPNs properties towards specific de-excitation pathways, which could have enhanced capabilities either as fluorescent probes or photothermal agents, in line with the desired end-user application and/or instrumental availability.

As to the capability of heat diffusion through the sample, **Figure 7** shows that all CPNs presented similar values, which were higher than 100% PEG-PLGA nanoparticles, independently of the type of PEG-PLGA or production condition. Therefore, the presence of PCPDBT embedded into the PEG-PLGA matrix contributed to a more rapid heat distribution through the sample. In other words, the CPNs can dissipate heat more easily than PEG-PLGA nanoparticles without PCPDTBT, which on the other hand, can sustain an increase in temperature for longer periods of time.

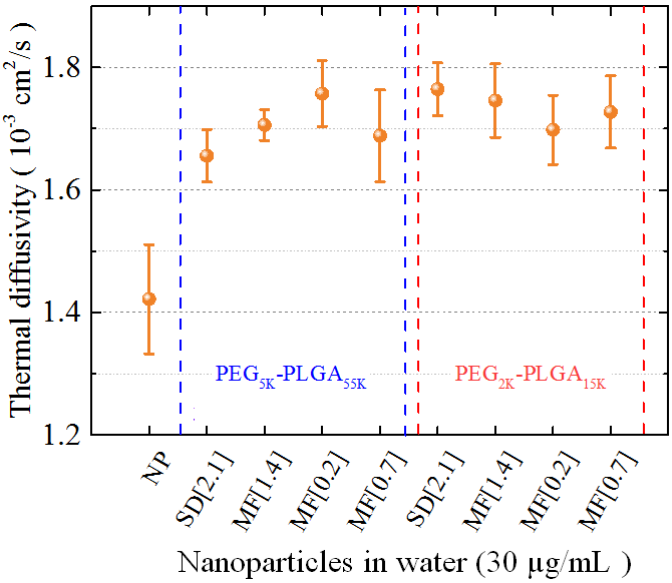

Figure 7. Thermal diffusivity of different CPNs and 100% PEG_{5k}-$PLGA_{55k}$ (NP) at 30 µg/mL total solids (1.4 µg/mL PCPDTBT + 28.6 µg/mL PEG-PLGA).

Overall, all PCPDTBT CPNs prepared in this study promoted similar heat diffusion though the sample, but the light-to-heat conversion efficiency was dependent on the preparation conditions. As the de-excitation mechanisms through luminescence emission and heat generation are complementary, CPNs with high light-to-heat conversion efficiency, such as MF1:14[0.2] containing PEG_{5k}-$PLGA_{55k}$, would therefore be a good candidate for photothermal therapy or photoacoustic imaging, but would perform less efficiently as a fluorescent probe for bioimaging. Conversely, microfluidics CPNs with low light-to-heat conversion efficiency, such as MF1:14[0.2] prepared with PEG_{2k}-$PLGA_{15k}$ and MF1:2[1.4] containing PEG_{5k}-$PLGA_{55k}$, would be potential candidates for luminescent-based applications. CPNs with intermediate heat generation capabilities, like the bulk formulations, could perform as dual-modality probes or

theranostic agents, which has been previously reported for PCPDTBT CPNs used both for fluorescence imaging and photothermal therapy.[12]

CONCLUSIONS

In conclusion, this work assessed the impact of preparation conditions and formulation on the photophysical properties of PCPDTBT nanoparticles with a particular focus on the efficiency of heat generation upon photoexcitation characterized by the TLS technique. To do so, PCPDTBT CPNs were generated by a traditional bulk method as well as microfluidics, using amphiphilic PEG-PLGA of different molecular weights. CPNs prepared by a traditional bulk method presented high production yields and comparable sizes irrespective of the molecular weight of PEG-PLGA. In contrast, the molecular weight of PEG-PLGA associated with the microfluidic production settings influenced the final product yield and the nanoparticle size of PCPDTBT CPNs. In all cases, we report absorption spectra which exhibited hypsochromic shifts when compared to PCPDTBT in solution, which can be attributed to the folding of the polymer chains and associated greater HOMO-LUMO bandgap. In turn, fluorescence emission spectra were bathochromically shifted, consistent with polymeric aggregation in the nanoparticles. Interestingly, this led to highly desirable large Stokes shifts. Under the same microfluidic settings (1:14[0.2]) PEG_{5k}-$PLGA_{55k}$ and PEG_{2k}-$PLGA_{15k}$ had contrasting effects on the heat generation capability of PCPDTBT, with the higher molecular weight copolymer enabling the best photothermal performance. In addition, TLS revealed that the presence of PCPDTBT embedded into the PEG-PLGA matrix resulted in increased heat diffusion through the sample, independently of the type of PEG-PLGA or production condition. Overall, this work shows that the conditions used for nanoparticle assembly, including production set-up and shell composition, play an important role in defining the thermo-

optical features of a CPN; this knowledge is crucial to guide the choice of potential candidates with optimized characteristics for biomedical applications. We also demonstrate the usefulness of the TLS technique to determine the light-to-heat conversion efficiency of CPNs.

ASSOCIATED CONTENT

Supporting Information.

TLS set up illustration; characterization of relevant TLS parameters; thermal diffusivity and thermal lens effect amplitude characterization of 100% PEG-PLGA nanoparticles; determination of linearity of fit based on the thermal lens signal amplitude under different laser powers (PDF).

AUTHOR INFORMATION

Corresponding Author

*Thais F. Abelha: Federal University of Mato Grosso do Sul, Institute of Physics, Campo Grande, Mato Grosso do Sul, 79070-900, Brazil. E-mail: thais.abelha@ufms.br

*Sandro M. Lima: Universidade Estadual de Mato Grosso do Sul, Grupo de Espectroscopia Óptica e Fototérmica, Dourados, Mato Grosso do Sul, 79804-970, Brazil. E-mail: smlima@uems.br

Present Addresses

†Federal University of Mato Grosso do Sul, Institute of Physics, Campo Grande, Mato Grosso do Sul, 79070-900, Brazil. E-mail: thais.abelha@ufms.br

Author Contributions

The manuscript was written through contributions of all authors. All authors have given approval to the final version of the manuscript.

Funding Sources

This study was financed in part by the Coordenação de Aperfeiçoamento de Pessoal de Nível Superior – Brasil (CAPES) – Finance Code 99999.000685/2013-05.

ACKNOWLEDGMENT

The Brazilian Government Program Science Without Borders for the full 4-year PhD scholarship and funding provided.

REFERENCES

(1) Qiu, Z.; Hammer, B. A. G.; Müllen, K. Conjugated Polymers – Problems and Promises. *Prog. Polym. Sci.* **2020**, *100*, 101179. https://doi.org/10.1016/j.progpolymsci.2019.101179.

(2) Fedatto Abelha, T.; Rodrigues Lima Caires, A. Light-Activated Conjugated Polymers for Antibacterial Photodynamic and Photothermal Therapy. *Adv. NanoBiomed Res.* **2021**, *1* (7), 2100012. https://doi.org/10.1002/anbr.202100012.

(3) Abelha, T. F.; Dreiss, C. A.; Green, M. A.; Dailey, L. A. Conjugated Polymers as Nanoparticle Probes for Fluorescence and Photoacoustic Imaging. *J. Mater. Chem. B* **2020**, *8* (4), 592–606. https://doi.org/10.1039/C9TB02582K.

(4) Xiao, L.; Chen, X.; Yang, X.; Sun, J.; Geng, J. Recent Advances in Polymer-Based Photothermal Materials for Biological Applications. *ACS Appl. Polym. Mater.* **2020**, *2* (10),

4273–4288. https://doi.org/10.1021/acsapm.0c00711.

(5) Yuan, H.; Wang, B.; Lv, F.; Liu, L.; Wang, S. Conjugated-Polymer-Based Energy-Transfer Systems for Antimicrobial and Anticancer Applications. *Adv. Mater.* **2014**, *26* (40), 6978–6982. https://doi.org/10.1002/adma.201400379.

(6) Hanack, M.; Behnisch, B.; Häckl, H.; Martinez-Ruiz, P.; Schweikart, K.-H. Influence of the Cyano-Group on the Optical Properties of Oligomeric PPV-Derivatives. *Thin Solid Films* **2002**, *417* (1–2), 26–31. https://doi.org/10.1016/S0040-6090(02)00591-6.

(7) Zhou, T.; Hu, R.; Wang, L.; Qiu, Y.; Zhang, G.; Deng, Q.; Zhang, H.; Yin, P.; Situ, B.; Zhan, C.; Qin, A.; Tang, B. Z. An AIE-Active Conjugated Polymer with High ROS-Generation Ability and Biocompatibility for Efficient Photodynamic Therapy of Bacterial Infections. *Angew. Chemie Int. Ed.* **2020**, *510010*, anie.201916704. https://doi.org/10.1002/anie.201916704.

(8) Greenham, N. C.; Samuel, I. D. W.; Hayes, G. R.; Phillips, R. T.; Kessener, Y. A. R. R.; Moratti, S. C.; Holmes, A. B.; Friend, R. H. Measurement of Absolute Photoluminescence Quantum Efficiencies in Conjugated Polymers. *Chem. Phys. Lett.* **1995**, *241* (1–2), 89–96. https://doi.org/10.1016/0009-2614(95)00584-Q.

(9) Abelha, T. F.; Phillips, T. W.; Bannock, J. H.; Nightingale, A. M.; Dreiss, C. A.; Kemal, E.; Urbano, L.; de Mello, J. C.; Green, M. A.; Dailey, L. A. Bright Conjugated Polymer Nanoparticles Containing a Biodegradable Shell Produced at High Yields and with Tuneable Optical Properties by a Scalable Microfluidic Device. *Nanoscale* **2017**, *9*, 2009–2019. https://doi.org/10.1039/C6NR09162H.

(10) Abelha, T. F.; Neumann, P. R.; Holthof, J.; Dreiss, C. A.; Alexander, C.; Green, M.; Dailey, L. A. Low Molecular Weight PEG–PLGA Polymers Provide a Superior Matrix for Conjugated Polymer Nanoparticles in Terms of Physicochemical Properties, Biocompatibility and Optical/Photoacoustic Performance. *J. Mater. Chem. B* **2019**, *7* (33), 5115–5124. https://doi.org/10.1039/C9TB00937J.

(11) Pu, K.; Shuhendler, A. J.; Jokerst, J. V.; Mei, J.; Gambhir, S. S.; Bao, Z.; Rao, J. Semiconducting Polymer Nanoparticles as Photoacoustic Molecular Imaging Probes in Living Mice. *Nat. Nanotechnol.* **2014**, *9* (3), 233–239. https://doi.org/10.1038/nnano.2013.302.

(12) Yoon, J.; Kwag, J.; Shin, T. J.; Park, J. J.; Lee, Y. M. Y.; Lee, Y. M. Y.; Park, J. J.; Heo, J.; Joo, C.; Park, T. J.; Yoo, P. J.; Kim, S. Nanoparticles of Conjugated Polymers Prepared from Phase-Separated Films of Phospholipids and Polymers for Biomedical Applications. *Adv. Mater.* **2014**, *26* (26), 4559–4564. https://doi.org/10.1002/adma.201400906.

(13) Lyu, Y.; Fang, Y.; Miao, Q.; Zhen, X.; Ding, D.; Pu, K. Intraparticle Molecular Orbital Engineering of Semiconducting Polymer Nanoparticles as Amplified Theranostics for in Vivo Photoacoustic Imaging and Photothermal Therapy. *ACS Nano* **2016**, *10* (4), 4472–4481. https://doi.org/10.1021/acsnano.6b00168.

(14) Würth, C.; Grabolle, M.; Pauli, J.; Spieles, M.; Resch-genger, U. Relative and Absolute Determination of Fluorescence Quantum Yields of Transparent Samples. *Nat. Protoc.* **2013**, *8* (8), 1535–1550. https://doi.org/10.1038/nprot.2013.087.

(15) Parker, C. A.; Rees, W. T. Correction of Fluorescence Spectra and Measurement of Fluorescence Quantum Efficiency. *Analyst* **1960**, *85* (1013), 587.

https://doi.org/10.1039/an9608500587.

(16) Crosby, G. A.; Demas, J. N. Measurement of Photoluminescence Quantum Yields. Review. *J. Phys. Chem.* **1971**, *75* (8), 991–1024. https://doi.org/10.1021/j100678a001.

(17) Jathoul, A. P.; Laufer, J.; Ogunlade, O.; Treeby, B.; Cox, B.; Zhang, E.; Johnson, P.; Pizzey, A. R.; Philip, B.; Marafioti, T.; Lythgoe, M. F.; Pedley, R. B.; Pule, M. a.; Beard, P. Deep in Vivo Photoacoustic Imaging of Mammalian Tissues Using a Tyrosinase-Based Genetic Reporter. *Nat. Photonics* **2015**, *9*, 239–246. https://doi.org/10.1038/nphoton.2015.22.

(18) Beard, P. Biomedical Photoacoustic Imaging. *Interface Focus* **2011**, *1* (4), 602–631. https://doi.org/10.1098/rsfs.2011.0028.

(19) Vargas, H.; Miranda, L. C. M. Photoacoustic and Related Photothermal Techniques. *Phys. Rep.* **1988**, *161* (2), 43–101. https://doi.org/10.1016/0370-1573(88)90100-7.

(20) Braslavsky, S. E. Glossary of Terms Used in Photochemistry, 3rd Edition (IUPAC Recommendations 2006). *Pure Appl. Chem.* **2007**, *79* (3), 293–465. https://doi.org/10.1351/pac200779030293.

(21) Gordon, J. P.; Leite, R. C. C.; Moore, R. S.; Porto, S. P. S.; Whinnery, J. R. Long-Transient Effects in Lasers with Inserted Liquid Samples. *J. Appl. Phys.* **1965**, *36* (1), 3–8. https://doi.org/10.1063/1.1713919.

(22) Bouchard, R. R.; Sahin, O.; Emelianov, S. S. Ultrasound-Guided Photoacoustic Imaging: Current State and Future Development. *IEEE Trans. Ultrason. Ferroelectr. Freq. Control* **2014**, *61* (3), 450–466. https://doi.org/10.1109/TUFFC.2014.2930.

(23) Ventura, M.; Silva, J. R.; Andrade, L. H. C.; Scorza Júnior, R. P.; Lima, S. M. Near-near-

Infrared Thermal Lens Spectroscopy to Assess Overtones and Combination Bands of Sulfentrazone Pesticide. *Spectrochim. Acta Part A Mol. Biomol. Spectrosc.* **2018**, *188*, 32–36. https://doi.org/10.1016/j.saa.2017.06.043.

(24) Baesso, M.; Bento, a.; Andrade, a.; Sampaio, J.; Pecoraro, E.; Nunes, L.; Catunda, T.; Gama, S. Absolute Thermal Lens Method to Determine Fluorescence Quantum Efficiency and Concentration Quenching of Solids. *Phys. Rev. B* **1998**, *57* (17), 10545–10549. https://doi.org/10.1103/PhysRevB.57.10545.

(25) Lima, S. M.; Souza, A. K. R.; Langaro, A. P.; Silva, J. R.; Costa, F. B.; Moraes, J. C. S.; Figueiredo, M. S.; Santos, F. A.; Baesso, M. L.; Nunes, L. A. O.; Andrade, L. H. C. Fluorescence Quantum Yield of Yb3+-Doped Tellurite Glasses Determined by Thermal Lens Spectroscopy. *Opt. Mater. (Amst).* **2017**, *63*, 19–25. https://doi.org/10.1016/j.optmat.2016.08.042.

(26) Figueiredo, M. S.; Santos, F. A.; Yukimitu, K.; Moraes, J. C. S.; Silva, J. R.; Baesso, M. L.; Nunes, L. A. O.; Andrade, L. H. C.; Lima, S. M. Luminescence Quantum Efficiency at 1.5 Mm of Er3+-Doped Tellurite Glass Determined by Thermal Lens Spectroscopy. *Opt. Mater. (Amst).* **2013**, *35* (12), 2400–2404. https://doi.org/10.1016/j.optmat.2013.06.041.

(27) Pereira, T. O.; Warzecha, M.; Andrade, L. H. C.; Silva, J. R.; Baesso, M. L.; McHugh, C. J.; Calvo-Castro, J.; Lima, S. M. True Absolute Determination of Photoluminescence Quantum Yields by Coupling Multiwavelength Thermal Lens and Photoluminescence Spectroscopy. *Phys. Chem. Chem. Phys.* **2020**, *22* (43), 25156–25164. https://doi.org/10.1039/D0CP03794J.

(28) Stephen E. Bialkowski; Astrath, N. G. C.; Proskurnin, M. A. *Photothermal Spectroscopy*

Methods, 2nd ed., 512; John Wiley & Sons, 2019.

(29) Daimon, M.; Masumura, A. Measurement of the Refractive Index of Distilled Water from the Near-Infrared Region to the Ultraviolet Region. *Appl. Opt.* **2007**, *46* (18), 3811. https://doi.org/10.1364/AO.46.003811.

(30) Dhankar, R.; Rathee, P.; Jain, A. K.; Arora, S.; Kumar, S.; Rath, G.; Saxena, A. K.; Sharma, P. R.; Goyal, A. K. HER-2 Targeted Immunonanoparticles for Breast Cancer Chemotherapy. *J. Appl. Pharm. Sci.* **2011**, *01* (03), 132–139.

(31) Gref, R.; Luck, M.; Quellec, P.; Marchand, M.; Dellacherie, E.; Harnisch, S.; Blunk, T.; Mulller, R. H. ' Stealth ' Corona-Core Nanoparticles Surface Modified by Polyethylene Glycol (PEG): Influences of the Corona (PEG Chain Length and Surface Density) and of the Core Composition on Phagocytic Uptake and Plasma Protein Adsorption. *Colloids Surfaces B Biointerfaces 18* **2000**, *18*, 301–313.

(32) Liu, X.; Atwater, M.; Wang, J.; Huo, Q. Extinction Coefficient of Gold Nanoparticles with Different Sizes and Different Capping Ligands. *Colloids Surfaces B Biointerfaces* **2007**, *58* (1), 3–7. https://doi.org/10.1016/j.colsurfb.2006.08.005.

(33) Zhou, T.; Wu, B.; Xing, D. Bio-Modified Fe3O4 Core/Au Shell Nanoparticles for Targeting and Multimodal Imaging of Cancer Cells. *J. Mater. Chem.* **2012**, *22* (2), 470–477. https://doi.org/10.1039/C1JM13692E.

(34) Schuster, M.; Wernicke, T.; Möckel, S. A.; Wellmann, P. J. Nanoparticles and Nanotechnology Determination of the Molar Extinction Coefficient of Colloidal Selenium for Optical Characterization of Stabilized Nanoparticulate Dispersions. *Int. J. Nanoparticles*

Nanotechnol. **2016**, *2* (1), 1–8.

(35) Khanbeigi, R. A.; Abelha, T. F.; Woods, A.; Rastoin, O.; Harvey, R. D.; Jones, M.-C.; Forbes, B.; Green, M. A.; Collins, H.; Dailey, L. A. Surface Chemistry of Photoluminescent F8BT Conjugated Polymer Nanoparticles Determines Protein Corona Formation and Internalization by Phagocytic Cells. *Biomacromolecules* **2015**, *16* (3), 733–742. https://doi.org/10.1021/bm501649y.

(36) Li, K.; Pan, J.; Feng, S. S.; Wu, A. W.; Pu, K. Y.; Liu, Y.; Liu, B. Generic Strategy of Preparing Fluorescent Conjugated-Polymer-Loaded Poly(DL-Lactide-Co-Glycolide) Nanoparticles for Targeted Cell Imaging. *Adv. Funct. Mater.* **2009**, *19* (22), 3535–3542. https://doi.org/10.1002/adfm.200901098.

(37) Kang, X.; Luo, C.; Wei, Q.; Xiong, C.; Chen, Q.; Chen, Y.; Ouyang, Q. Mass Production of Highly Monodisperse Polymeric Nanoparticles by Parallel Flow Focusing System. *Microfluid. Nanofluidics* **2013**, *15* (3), 337–345. https://doi.org/10.1007/s10404-013-1152-6.

(38) Lim, J.-M.; Bertrand, N.; Valencia, P. M.; Rhee, M.; Langer, R.; Jon, S.; Farokhzad, O. C.; Karnik, R. Parallel Microfluidic Synthesis of Size-Tunable Polymeric Nanoparticles Using 3D Flow Focusing towards in Vivo Study. *Nanomedicine* **2014**, *10* (2), 401–409. https://doi.org/10.1016/j.nano.2013.08.003.

(39) Duan, X.; Li, Y. Physicochemical Characteristics of Nanoparticles Affect Circulation, Biodistribution, Cellular Internalization, and Trafficking. *Small* **2013**, *9* (9–10), 1521–1532. https://doi.org/10.1002/smll.201201390.

(40) Neumann, P. R.; Erdmann, F.; Holthof, J.; Hädrich, G.; Green, M.; Rao, J.; Dailey, L. A. Different PEG-PLGA Matrices Influence In Vivo Optical/Photoacoustic Imaging Performance and Biodistribution of NIR-Emitting π -Conjugated Polymer Contrast Agents. *Adv. Healthc. Mater.* **2021**, *10* (4), 2001089. https://doi.org/10.1002/adhm.202001089.

(41) Kandel, P. K.; Fernando, L. P.; Ackroyd, P. C.; Christensen, K. A. Incorporating Functionalized Polyethylene Glycol Lipids into Reprecipitated Conjugated Polymer Nanoparticles for Bioconjugation and Targeted Labeling of Cells. *Nanoscale* **2011**, *3* (3), 1037–1045. https://doi.org/10.1039/c0nr00746c.

(42) Clogston, J. D.; Patri, A. K. Zeta Potential Measurement. In *Characterization of Nanoparticles Intended for Drug Delivery*; 2011; pp 63–70. https://doi.org/10.1007/978-1-60327-198-1_6.

(43) Haggag, Y.; Abdel-Wahab, Y.; Ojo, O.; Osman, M.; El-Gizawy, S.; El-Tanani, M.; Faheem, A.; McCarron, P. Preparation and in Vivo Evaluation of Insulin-Loaded Biodegradable Nanoparticles Prepared from Diblock Copolymers of PLGA and PEG. *Int. J. Pharm.* **2016**, *499* (1–2), 236–246. https://doi.org/10.1016/j.ijpharm.2015.12.063.

(44) Kaszuba, M.; Corbett, J.; Watson, F. M.; Jones, A. High-Concentration Zeta Potential Measurements Using Light-Scattering Techniques. *Philos. Trans. A. Math. Phys. Eng. Sci.* **2010**, *368*, 4439–4451. https://doi.org/10.1098/rsta.2010.0175.

(45) Pamujula, S.; Hazari, S.; Bolden, G.; Graves, R. A.; Chinta, D. D.; Dash, S.; Kishore, V.; Mandal, T. K. Cellular Delivery of PEGylated PLGA Nanoparticles. *J. Pharm. Pharmacol.* **2012**, *64* (1), 61–67. https://doi.org/10.1111/j.2042-7158.2011.01376.x.

(46) Schwartz, B. J. Conjugated Polymers as Molecular Materials: How Chain Conformation and Film Morphology Influence Energy Transfer and Interchain Interactions. *Annu. Rev. Phys. Chem.* **2003**, *54* (1), 141–172. https://doi.org/10.1146/annurev.physchem.54.011002.103811.

(47) Nguyen, T.-Q.; Doan, V.; Schwartz, B. J. Conjugated Polymer Aggregates in Solution: Control of Interchain Interactions. *J. Chem. Phys.* **1999**, *110* (8), 4068. https://doi.org/10.1063/1.478288.

(48) Zhang, X.; Bloch, S.; Akers, W.; Achilefu, S. Near-Infrared Molecular Probes for in Vivo Imaging. *Curr. Protoc. Cytom.* **2012**, *60*, 1–28. https://doi.org/10.1002/0471142956.cy1227s60.

(49) Smith, A. M.; Mancini, M. C.; Nie, S. Bioimaging: Second Window for in Vivo Imaging. *Nat. Nanotechnol.* **2009**, *4* (11), 710–711. https://doi.org/10.1038/nnano.2009.326.

(50) Hashim, Z.; Howes, P.; Green, M. Luminescent Quantum-Dot-Sized Conjugated Polymer Nanoparticles: Nanoparticle Formation in a Miniemulsion System. *J. Mater. Chem.* **2011**, *21* (6), 1797–1803. https://doi.org/10.1039/c0jm02935a.

(51) Hashim, Z.; Green, M.; Chung, P. H.; Suhling, K.; Protti, A.; Phinikaridou, A.; Botnar, R.; Khanbeigi, R. A.; Thanou, M.; Dailey, L. A.; Commander, N. J.; Rowland, C.; Scott, J.; Jenner, D. Gd-Containing Conjugated Polymer Nanoparticles: Bimodal Nanoparticles for Fluorescence and MRI Imaging. *Nanoscale* **2014**, *6* (14), 8376–8386. https://doi.org/10.1039/C4NR01491J.

(52) Wu, C.; Bull, B.; Szymanski, C.; Christensen, K.; McNeill, J. Multicolor Conjugated

Polymer Dots for Biological Fluorescence Imaging. *ACS Nano* **2008**, *2* (11), 2415–2423. https://doi.org/10.1021/nn800590n.

(53) Seybold, P. G.; Gouterman, M.; Callis, J. Calorimetric, Photometric and Lifetime Determinations of Fluorescence Yields of Fluorescein Dyes. *Photochem. Photobiol.* **1969**, *9* (3), 229–242. https://doi.org/10.1111/j.1751-1097.1969.tb07287.x.

(54) Hunter, T. F. Measuring Weak Absorption Spectra. *Nature* **1979**, *280*, 357–358.

(55) Caspar, J. V.; Meyer, T. J. Application of the Energy Gap Law to Nonradiative, Excited-State Decay. *J. Phys. Chem.* **1983**, *87* (6), 952–957. https://doi.org/10.1021/j100229a010.

For Table of Contents Only